Available online at www.sciencedirect.com
ScienceDirect
Journal of Power Sources 172 (2007) 198–208
JOURNAL OF POWER SOURCES
www.elsevier.com/locate/jpowsour

# A membraneless microscale fuel cell using non-noble catalysts in alkaline solution

Woosuk Sung [a], Jin-Woo Choi [a,b,*]

[a] *Department of Electrical and Computer Engineering, Louisiana State University, Baton Rouge, LA 70803, USA*
[b] *Center for Advanced Microstructures and Devices, Louisiana State University, Baton Rouge, LA 70803, USA*

Received 24 May 2007; received in revised form 2 July 2007; accepted 3 July 2007
Available online 17 July 2007

**Abstract**

This paper presents the development of a novel liquid-based microscale fuel cell using non-noble catalysts in an alkaline solution. The developed fuel cell is based on a membraneless structure. The operational complications of a proton exchange membrane lead the development of a fuel cell with the membraneless structure. Non-noble metals with relatively mild catalytic activity, nickel hydroxide and silver oxide, were employed as anode and cathode catalysts to minimize the effect of cross-reactions with the membraneless structure. Along with nickel hydroxide and silver oxide, methanol and hydrogen peroxide were used as a fuel at anode and an oxidant at cathode. With a fuel mixture flow rate of 200 $\mu l\,min^{-1}$, a maximum output power density of 28.73 $\mu W\,cm^{-2}$ was achieved. The developed fuel cell features no proton exchange membrane, inexpensive catalysts, and simple planar structure, which enables high design flexibility and easy integration of the microscale fuel cell into actual microfluidic systems and portable applications.


*Keywords:* Fuel cell; Membraneless; Methanol; Hydrogen peroxide; Non-noble catalyst

## 1. Introduction

A fuel cell is an electrochemical device that converts chemical energy into electrical energy. Recently, there has been a rapidly growing demand for miniaturized power sources for portable electronic telecommunication and computing devices such as mobile phones, personal digital assistants, and laptop computers [1]. Battery technology has advanced significantly over the years so that such needs have been generally met by lithium ion [2] and nickel metal hydride-based rechargeable batteries [3]. However, with the ever-increasing energy demand in recent years, the power available from the rechargeable batteries may become insufficient to keep pace with the power required from the portable devices [4,5]. As an alternative, miniaturized fuel cells have attracted wide attention due to their high energy density and continuous operation capability by refueling [6]. Among diverse fuels available in either gas or liquid phase, liquid-based fuel cells are preferred because liquid phase fuels like methanol can be more readily distributed and easily stored than gas phase hydrogen [7]. In contrast to rechargeable batteries requiring periods of hours to be replenished, a liquid-based microscale fuel cell can be renewed in a few seconds by replacing a spent fuel cartridge. Furthermore, liquid fuels have a higher energy density than gaseous hydrogen [4,5]. Consequently, there have been a number of reports on the development and demonstration of liquid-based microscale fuel cells as an efficient and compact power source for powering portable electronic devices and microelectromechanical systems (MEMS) [8–13].

Although the liquid-based microscale fuel cells have shown the feasibility of miniaturized power sources, there are a few issues that need to be addressed. One of the critical limitations is a proton exchange membrane. A proton exchange membrane is considered as an essential component to realize a fuel cell as it allows protons to pass through from the anode to the cathode while preventing fuel species from reaching the cathode. However, there is a critical requirement on the thickness of the membrane that could affect design flexibility of a microscale fuel cell. In principle, a thinner membrane would reduce the transport time of a charge carrier and thus increase the reaction rate. However, a thinner membrane may also exhibit higher fuel

* Corresponding author. Tel.: +1 225 578 8764; fax: +1 225 578 5200.
*E-mail address:* choi@ece.lsu.edu (J.-W. Choi).

0378-7753/$ – see front matter © 2007 Elsevier B.V. All rights reserved.
doi:10.1016/j.jpowsour.2007.07.012

crossover that leads a loss in fuel cell performance. The optimal thickness of the membrane is desired in order to achieve the maximum fuel cell performance. In addition, segregation of fuel and oxidant compartments by the membrane could make the overall structure of a microscale fuel cell complicated [14]. Besides, a water-rich environment, particularly in a liquid-based fuel cell, leads to the swelling of the membrane [15]. The dimensional instability of the membrane would have a deleterious effect on the dependability of a fuel cell. Gaseous by-product at the anode and water dews at the cathode, which would block fuel and oxidant from anode and cathode surfaces, is another limitation of liquid-based microscale fuel cells. This transport blockage would be more critical in channels of small dimensions as the gaseous by-product could form bubbles and impede fuel flow in the microfluidic channels [16].

For these reasons, in recent years, a few membraneless fuel cells have been developed and reported [17–20]. The reported membraneless fuel cells utilized a laminar flow in microchannels to segregate fuel and oxidant. Choban et al. [17,18] reported laminar flow-based membraneless fuel cells. Cohen et al. [19] also demonstrated membraneless microchannel fuel cells. Microchannels were formed by silicon bulk etching and a laminar flow segregated fuel and oxidant.

The main motivation of this work is to develop a liquid-based microscale fuel cell with a membraneless structure that can overcome the design limitations caused by the use of the proton exchange membrane. In addition, a laminar flow control is not necessary in this work so a simple microfluidic structure can be achievable. Due to the absence of a membrane, the distance between anode and cathode will not be restricted by the membrane thickness any more. The distance between anode and cathode determines diffusion length of reacting species. A shorter diffusion length is expected to cause a faster diffusion time, thereby expediting the electrochemical reactions and thus increasing the fuel cell output power. However, in return for such merits of a membraneless structure, its expected drawbacks are that fuel and oxidant species would mix and reach the opposite electrode, undesirably allowing cross-reactions. Even though this tangible loss may be offset to a certain degree by the potential gain from a reduced diffusion length of reacting species, it cannot be a radical solution. Rather, an alternative approach to this problem is to choose appropriate catalysts for use in a membraneless structure.

Non-noble metals with relatively mild catalytic activity, nickel hydroxide and silver oxide, are selected as anode and cathode catalysts to minimize the effect of cross-reactions that may be occurred with the membraneless structure and the use of a fuel mixture. Along with nickel hydroxide ($Ni(OH)_2$) and silver oxide (AgO), methanol and hydrogen peroxide are used as a fuel at anode and an oxidant at cathode as illustrated in Fig. 1.

## 2. Reaction mechanism

The operation of the fuel cell in this work is based on the anodic oxidation of methanol ($CH_3OH$) in combination with the cathodic reduction of hydrogen peroxide ($H_2O_2$) [21]. Methanol and hydrogen peroxide are catalyzed by nickel hydroxide and silver oxide, respectively. Additionally, due to the membraneless structure of the fuel cell, methanol and hydrogen peroxide could mix and reach to both electrodes. As a result, some cross-reactions would occur at both electrodes such that hydrogen peroxide could be catalyzed by nickel hydroxide while methanol could be catalyzed by silver oxide.

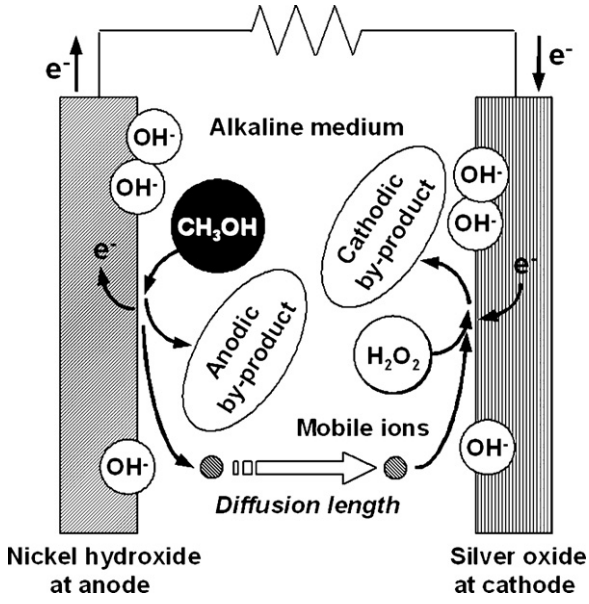


Fig. 1. Schematic illustration of the fuel cell using nickel hydroxide and silver oxide as catalysts. The distance between anode and cathode determines diffusion length of a charge carrier. In this reaction mechanism scheme, mobile ions are assumed to be cations to show the transport direction of mobile ions.

### 2.1. Electrochemical reactions at silver oxide

There have been several reports on the reduction of hydrogen peroxide on silver-based materials [22–25]. Bianchi et al. [22] reported that hydrogen peroxide was decomposed into oxygen and hydroxyl ions, and the produced oxygen was then reduced at silver oxide in an alkaline solution. Similar observation was also reported by Iwakura et al. [23] whose results showed that hydrogen peroxide reduction involved hydrogen peroxide decomposition followed by oxygen reduction. Another reaction model was proposed by Honda et al. [24] who explained the reduction of hydrogen peroxide is associated with the molecular form of hydrogen peroxide ($H_2O_2$) and the ionic form of hydrogen peroxide ($HO_2^-$). It was explained that the dissociation of hydrogen peroxide resulted in the coexistence of two different forms of hydrogen peroxide: $H_2O_2$ and $HO_2^-$. This reaction is reversible so that both dissociation and recombination occur at the same rate. The reduction of oxygen that was produced by the oxidation of ionic hydrogen peroxide ($HO_2^-$) can be negligible because the rate of oxygen reduction is much slower than the rate of hydrogen peroxide ($H_2O_2$) reduction [24]. More recently, Savinova et al. [25] also suggested that the reaction mechanism of hydrogen peroxide reduction that the rate of hydrogen peroxide reduction was strongly affected by the oxidation state of sliver in an alkaline solution. Although there is a contradiction

regarding detailed reaction mechanisms in the literature [22–25], two catalytic reactions are known to be combined in hydrogen peroxide reduction on silver oxide in an alkaline solution. One is the decomposition of hydrogen peroxide into oxygen and water [26]. This reaction is catalyzed by silver and takes place more rapidly in an alkaline solution [27]. The other is the reduction of hydrogen peroxide to water [26]. Several catalysts, such as platinum, palladium, iridium, silver, and a combination of these, were shown to be electroactive for the reduction of hydrogen peroxide. Unfortunately, however, these metals are also known to decompose hydrogen peroxide [28]. Thus, $H_2O_2$ reduction is accompanied with $H_2O_2$ decomposition if silver is employed as a catalyst. Depending on the electrons involved, hydrogen peroxide decomposition can be either chemical or electrochemical. In contrast to the electrochemical decomposition of $H_2O_2$ and the reduction of $H_2O_2$, the chemical decomposition of $H_2O_2$ is almost negligible in electron-consuming reduction reactions because it involves no electron transfer [28].

In addition to the reduction of hydrogen peroxide, the electrochemical reaction of methanol on silver-based materials also needs to be considered as it is probable with the membraneless structure. Although silver has been used as a catalyst for the oxidation of methanol to produce formaldehyde ($CH_2O$) on a large scale, this process requires high temperatures, usually 600–700 °C, for high conversion efficiency [29,30]. Thus, such reactions cannot occur at considerable rates in fuel cell operation at room temperature.

### 2.2. Electrochemical reactions at nickel hydroxide

Several studies on the oxidation of alcohols at nickel-based materials have been reported [31,32]. Fleischmann et al. [31] reported that most of the applied organic compounds including amines and alcohols were oxidized at the same potential where the nickel surface became oxidized to nickel oxyhydroxide (NiOOH). NiOOH was therefore assumed to be a catalyst for the oxidation of the organic compounds. Taraszewska and Roslonek [32] and El-Shafei [33] investigated the oxidation of methanol at a nickel hydroxide/glassy carbon ($Ni(OH)_2$/GC) electrode by cyclic voltammetry. The effects of methanol concentration and scan rate on methanol oxidation were experimentally studied. The cyclovoltammograms in their studies also demonstrated the relationship between the oxidation of methanol and the formation of NiOOH. More recently, Abdel Rahim et al. [34] observed that as voltammetry-cycling progressed, the current for methanol oxidation decreased and the potential for methanol oxidation slightly shifted toward less positive potentials, which indicated a loss of catalytic activity of the electroplated nickel/graphite electrode used. Despite disagreements with detailed reaction mechanisms in the literature [31–34], the oxidation of methanol is based on the nickel hydroxide cycling between two phases: $Ni(OH)_2$ and NiOOH. $Ni(OH)_2$ and NiOOH can be formed on the nickel surface in an alkaline solution and there exist two different forms of nickel hydroxide. They are denoted as β-$Ni(OH)_2$ and α-$Ni(OH)_2$, which can be oxidized to β-NiOOH and γ-NiOOH, respectively [35–37]. Although the mechanism for such phase transformation is not clearly understood, more electrons can be exchanged with α-$Ni(OH)_2$ compared to β-$Ni(OH)_2$ because the oxidation state of γ-NiOOH is higher than that of β-NiOOH [36]. Therefore, α-$Ni(OH)_2$ is expected to be a better electroactive material for the oxidation of methanol [37]. However, α-$Ni(OH)_2$ transforms into β-$Ni(OH)_2$ in an alkaline solution, resulting in degradation of electrochemical properties [37]. Nickel hydroxide is thus required to be stabilized to make use of it as a catalyst for the oxidation of methanol.

Aside from the oxidation of methanol, the electrochemical reaction of hydrogen peroxide on nickel-based materials should also be considered as it is probable with the membraneless structure. However, very few reports were found regarding the electrochemical reaction of $H_2O_2$ on nickel-based materials, particularly in an alkaline solution. Although Hall et al. have recently reported the mechanism of hydrogen peroxide oxidation on several electrodes including platinum [38] and nickel [39], their results are not directly applicable to the electrochemical reaction of $H_2O_2$ on nickel-based materials in an alkaline solution because the results were obtained in a neutral electrolyte.

## 3. Macroscale fuel cell test

Prior to fabrication of a microscale fuel cell, the methanol and hydrogen peroxide fuel cell concept was experimentally validated through a macroscale fuel cell test. Besides, the effect of operational conditions on the fuel cell output was examined including the catalyst surface conditions, fuel mixture composition, and distance between anode and cathode.

### 3.1. Catalyst and electrode preparation

Nickel hydroxide was prepared through nickel electrodeposition followed by electrochemical oxide formation. A nickel plate as an anode and a thin chromium/gold film (200 Å/3000 Å) on a glass substrate as a cathode were immersed in the nickel sulfate-based electrolyte. The current density of 5 mA $cm^{-2}$ was applied to an electrode area of 6.45 $cm^2$ for 20 min, resulting in the film thickness of 2 μm. In order to form nickel hydroxide after electroplating, the electroplated nickel was voltammetry-cycled within the potential range of −1.2 to 0.6 V with respect to a silver/silver chloride (Ag/AgCl) reference electrode in 1 M potassium hydroxide (KOH) at a scan rate of 10 mV $s^{-1}$ for 80 times [40,41].

Silver was also prepared by electroplating. For silver electroplating, a silver plate as an anode and a thin chromium/gold film (200 Å/3000 Å) on a glass substrate as a cathode were immersed in a commercially available silver electroplating solution (Cyless Silver, Technic, Inc., Cranston, RI). The current density of 3 mA $cm^{-2}$ was applied to an electrode area of 6.45 $cm^2$ for 15 min, resulting in the film thickness of 2 μm. After electroplating, no further treatment was conducted other than immersion of the electroplated silver in 1 M KOH to form silver oxide.

### 3.2. The stability of the electrodes

The macroscale fuel cell test was first carried out to stabilize the anode catalyst, nickel hydroxide, which is known to undergo the degradation of electrochemical properties due to the phase transformation in an alkaline solution [37]. The fuel mixture used in this experiment was composed of 0.1 M potassium hydroxide, 1 M methanol, and 0.025 M hydrogen peroxide. In order to maintain the concentration of these reactants during the experiment, the fuel mixture was replenished at a rate of 10 ml $min^{-1}$ using a syringe pump (PHD2000, Harvard Apparatus, Hamden, CT). The electrical measurement was provided by FieldPoint modules (FP-AI-100 and -110, National Instruments, Dallas, TX) along with LabVIEW (LabVIEW 7 Express, National Instruments, Dallas, TX).

The catalysts in the fuel cell were characterized by observing fuel cell output voltages and currents in the following order. First, the anode and cathode potentials were measured (versus Ag/AgCl) in the fuel mixture. At this point, the current–voltage measurement could be unreliable because the catalysts were unstable due to the phase transformation of nickel hydroxide in an alkaline solution. So, the output current was measured with a load resistance of 100 Ω until the current became stable. After the output current was stabilized, the anode and cathode potentials were measured again (versus Ag/AgCl), and subsequently, the output voltage and current were measured with various external loads.

As shown in Fig. 2, the output current continuously decreased for 5–6 h, and then settled at stabilized values. It is believed that the observed decline in the output current was caused by the aging effect of nickel hydroxide at the anode [36]. It was reported that the phase transformation of nickel hydroxide in an alkaline solution caused the degradation of electrochemical properties [37]. Once the electrodes were stabilized, the measured half-cell potential of the stabilized nickel hydroxide electrode remained unchanged even after testing the fuel cell with a 100 Ω load resistance more than 8 h. Silver oxide at the cathode was demonstrated to be relatively stable with a few evidences. The measured potential of the chemically formed silver oxide electrode remained unvaried during fuel cell operation. Also, it was observed that the fuel cell output current was stabilized as long as the nickel hydroxide at the anode became stable regardless of the condition of silver oxide at the cathode.

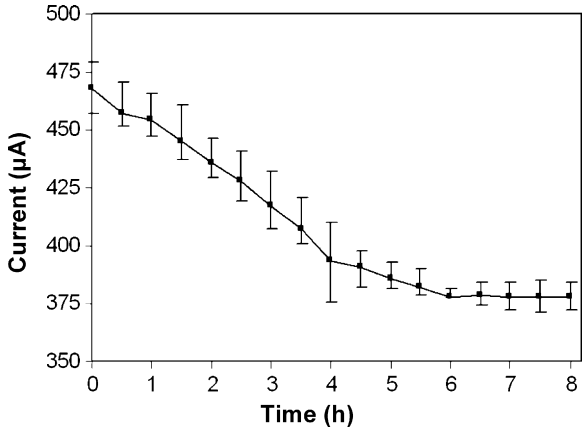


Fig. 2. Aging effect of the anode catalyst (nickel hydroxide) on the fuel cell output current. The cathode catalyst was silver oxide. The output current was measured with a 100 Ω load resistance for 8 h. Three pairs of electrode samples (6.45 $cm^2$) were tested. Three sets of the output current were averaged and then plotted with an error bar. The fuel mixture of 0.1 M KOH + 1 M $CH_3OH$ + 0.025 M $H_2O_2$ (65 ml) was supplied at a rate of 10 ml $min^{-1}$. Distance between anode and cathode was 20 mm.

### 3.3. Half-cell characterization

The concentration of hydroxyl ions plays an important role in the oxidation of nickel and silver, which leads to nickel hydroxide and silver oxide, respectively. The electrons released from the oxidation of nickel develop the anode potential while the electrons generated from the oxidation of silver develop the cathode potential, excluding minor influences from the other reactants. In this respect, the potential at the anode and cathode was measured (versus Ag/AgCl) for different $OH^-$ concentrations. The measured anode and cathode potentials (versus Ag/AgCl) are shown in Fig. 3. For both anode and cathode, the potential decreased as $OH^-$ concentration increased. More hydroxyl ions can produce

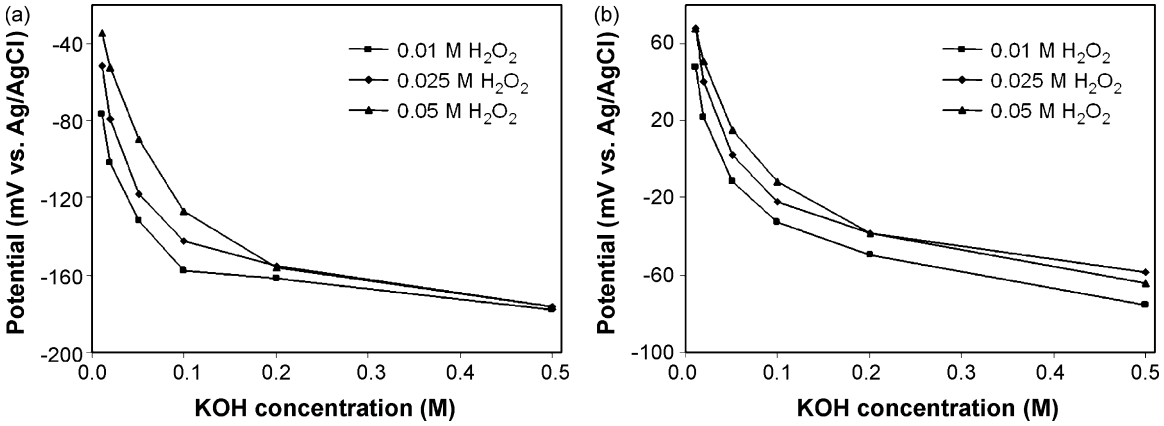


Fig. 3. Effect of KOH and $H_2O_2$ concentrations: (a) half-cell potential at the anode and (b) half-cell potential at the cathode. $CH_3OH$ concentration was fixed to 1 M. Half-cell potentials were measured with respect to an Ag/AgCl reference electrode. The anode catalyst was nickel hydroxide and the cathode catalyst was silver oxide. Temperature was 22.5 °C.

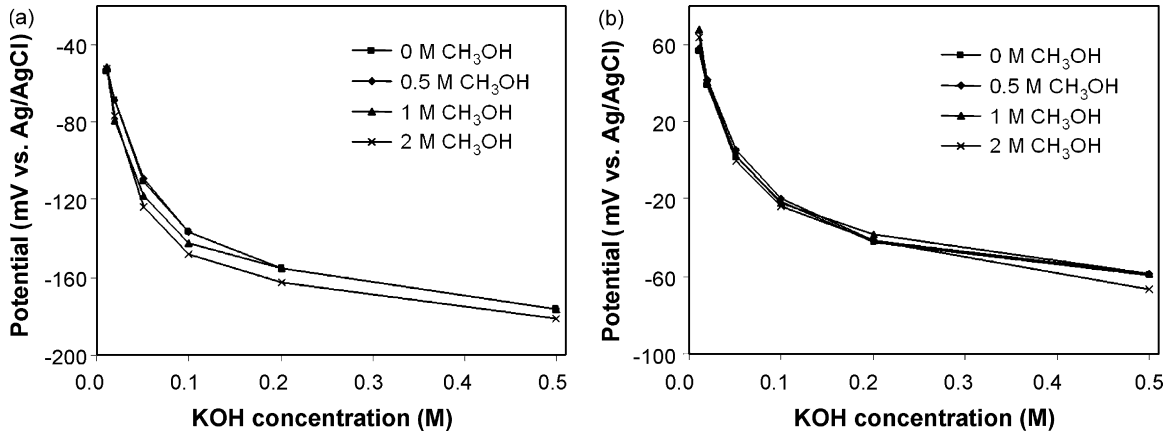


Fig. 4. Effect of KOH and $CH_3OH$ concentrations: (a) half-cell potential at the anode and (b) half-cell potential at the cathode. $H_2O_2$ concentration was fixed to 0.025 M. Half-cell potentials were measured with respect to an Ag/AgCl reference electrode. The anode catalyst was nickel hydroxide and the cathode catalyst was silver oxide. Temperature was 22.5 °C.

more electrons and hence develop a greater potential (versus Ag/AgCl), which is consistent with the nickel oxidation reaction at the anode [31,34]:

$$Ni + 2OH^- \rightarrow Ni(OH)_2 + 2e^- \quad (1)$$

$$Ni(OH)_2 + OH^- \rightarrow NiOOH + H_2O + e^- \quad (2)$$

and the silver oxidation reaction at the cathode [23,24]:

$$2Ag + 2OH^- \rightarrow Ag_2O + H_2O + 2e^- \quad (3)$$

The dependence of the anode and cathode potential on $OH^-$ concentration became weak for $OH^-$ concentrations higher than 0.2 M.

The effect of $H_2O_2$ concentrations on the half-cell potential at the anode and cathode is also shown in Fig. 4. For both anode and cathode, the potential increased as $H_2O_2$ concentration increased, which indicates that hydrogen peroxide led to undesirable reduction reactions (electron-consuming) even at the anode. Thus, for both electrodes, more hydrogen peroxide can lead to a faster hydrogen peroxide reduction reaction, which in turn consumes more electrons and hence develops a smaller potential (versus Ag/AgCl). However, similar to $OH^-$ concentration dependence, $H_2O_2$ concentration dependence of the half-cell potential of anode and cathode became less sensitive for $OH^-$ concentrations higher than 0.2 M.

Subsequently, $CH_3OH$ concentration dependence of the anode and cathode potentials was also investigated in the same manner. At the anode, the half-cell potential slightly decreased as the $CH_3OH$ concentration increased, as shown in Fig. 4. By contrast, at the cathode, the half-cell potential was almost insensitive to $CH_3OH$ concentration for the $OH^-$ concentrations considered.

### 3.4. The optimal composition of fuel mixture composition

The effect of reactant concentration on the fuel cell output was also experimentally studied to determine the optimal composition of a fuel mixture. Seventy two combinations of reactant concentration were applied: six KOH concentrations were applied as 0.01, 0.02, 0.05, 0.1, 0.2, and 0.5 M; four $CH_3OH$ concentrations were applied as 0, 0.5, 1, and 2 M; and three $H_2O_2$ concentrations were applied as 0.01, 0.025, and 0.05 M. The possible combinations including either 0 M KOH or 0 M $H_2O_2$ were not applied because the fuel cell output could not be stable without such reactants.

To determine the optimal composition of a fuel mixture, the current–voltage measurement was carried out with different external loads. The distance between the anode and cathode was maintained to 20 mm. The obtained maximum output powers with respect to the applied combinations of reactant concentration are presented in Fig. 5. As the amount of reactants increased in the ratio of 1:4:40 ($H_2O_2$:KOH:$CH_3OH$), the maximum output power increased. The highest output power density (5.02 $\mu W\,cm^{-2}$) was achieved with the fuel mixture of 0.2 M hydroxyl ions, 2 M methanol, and 0.05 M hydrogen peroxide. Consequently, a relative amount of reactants was found to be a more critical issue than their absolute amount. For a fixed ratio of 1:4:40 ($H_2O_2$:KOH:$CH_3OH$), however, an absolute amount of reactants also had an effect on the maximum output power. The maximum output power increased as the amount of reactants increased, maintaining the fuel mixture ratio of 1:4:40 ($H_2O_2$:KOH:$CH_3OH$). However, this dependence became weak for $CH_3OH$ concentrations larger than 2 M. Further, the 3 and 4 M $CH_3OH$-based fuel mixtures underwent relatively unstable output currents and showed a longer transient time compared to the 2 M $CH_3OH$-based fuel mixture. Considering the magnitude and stability of the fuel cell output, the optimal composition of a fuel mixture was determined to be 0.2 M hydroxyl ions, 2 M methanol, and 0.05 M hydrogen peroxide.

### 3.5. The distance effect on the fuel cell output

Based on the stabilized catalyst and optimized fuel mixture, the macroscale fuel cell test was conducted for different distances between the anode and cathode in order to find the

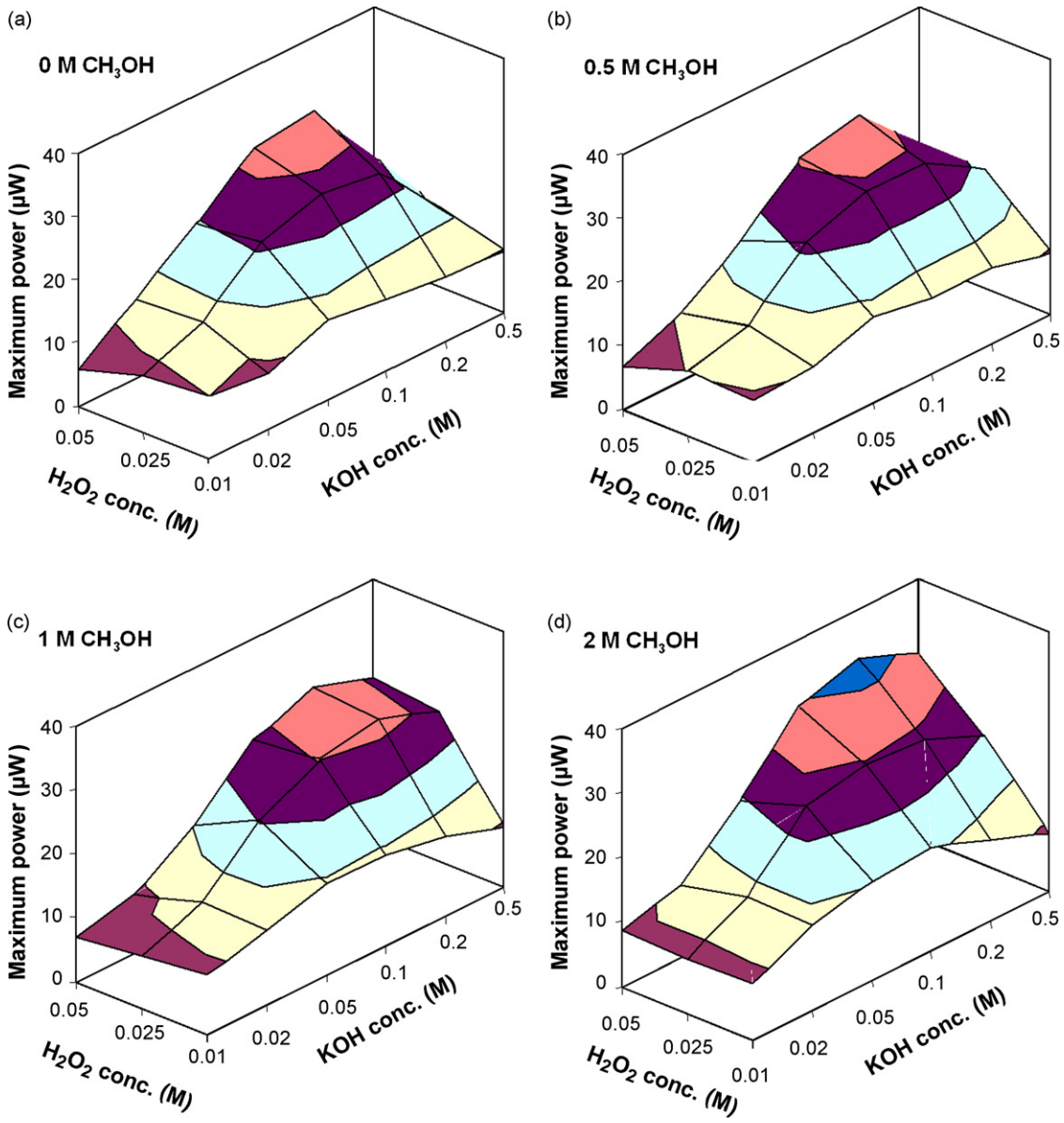


Fig. 5. Effect of various combinations of reactant concentrations on the maximum output power for: (a) 0 M methanol; (b) 0.5 M methanol; (c) 1 M methanol, and (d) 2 M methanol. The output voltage and current were measured with various external loads. The anode catalyst was nickel hydroxide and the cathode catalyst was silver oxide (6.45 $cm^2$). Distance between anode and cathode was 20 mm and temperature was 22.5 °C.

potential benefit from a reduced diffusion length of reacting species moving between the anode and cathode. The distance between anode and cathode was set from 1 to 100 mm. The output voltage and current were measured with various load resistances for different distances between the anode and cathode. As the distance between the anode and cathode decreased, the maximum output power increased as shown in Fig. 6. Considering the role of a charge carrier, a shorter diffusion length is believed to give a faster electrochemical reaction because the diffusion time of reacting species would be shorter. Therefore, more reactions can take place at a given time, which increases the total number of charges involving the electrochemical reactions at the anode and cathode. This finding provides a good evidence of the presence of a charge carrier moving between the anode and cathode in the fuel mixture to complete redox reactions of the fuel cell. The transport time of reacting species is shorter as the distance between electrodes is narrower so that the electrochemical reaction rate increases.

## 4. Microscale fuel cells

Depending on the distance effect demonstrated at the macroscale level, a microscale fuel cell was developed in order to further extend the distance effect to a microscale level that enables microscale diffusion lengths of reacting species. Four different designs of the microscale fuel cell were prepared to examine the distance effect between the anode and cathode on the fuel cell output. In addition, the microfluidic behavior of the microscale fuel cell was also characterized under different fuel mixture flow rates.

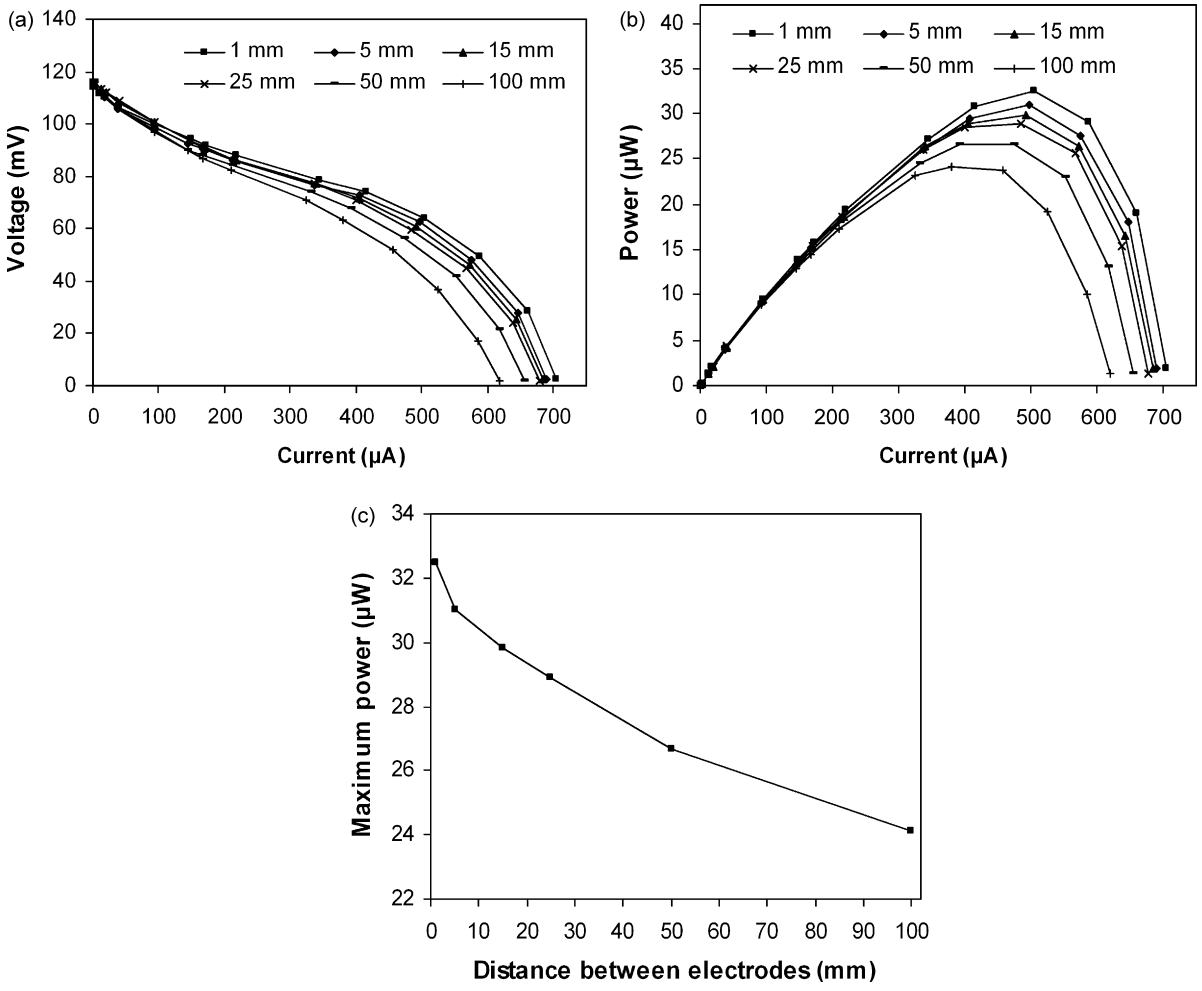


Fig. 6. Effect of distance between anode and cathode on the fuel cell output power: (a) the output voltage vs. the output current, (b) the output power vs. the output current, and (c) the maximum output power vs. the distance between electrodes. The output voltage and current were measured with various external loads. The anode catalyst was nickel hydroxide and the cathode catalyst was silver oxide (6.45 $cm^2$). The fuel mixture of 0.1 M KOH + 1 M $CH_3OH$ + 0.025 M $H_2O_2$ (65 ml) was supplied at a rate of 10 ml $min^{-1}$. Distance between anode and cathode was 20 mm. Temperature was 22.5 °C.

### *4.1. Design considerations*

The developed microscale fuel cell is based on a planar and membraneless structure. Thus, electrodes can be arranged on the same plane without a proton exchange membrane, so that the fuel cell dimensions can be flexibly adjusted to meet specific design needs. Moreover, since a fuel mixture is applied to the anode and cathode, a laminar flow control is not necessary and a simple microfluidic structure can be allowed. For the planar configuration, interdigitated microelectrodes were employed as the anode and cathode as illustrated in Fig. 7. Spacing between anodes and cathodes was determined by photolithography. Four different distances between anode and cathode, 10, 20, 50, and 100 μm, were prepared and tested for comparison. In each design, the anode and cathode area was unchanged to 1.35 $mm^2$.

### *4.2. Fabrication of microscale fuel cells*

The microscale fuel cells were fabricated on a glass substrate. The glass substrate was first carefully cleaned in a piranha etching solution of 70 vol.% sulfuric acid to 30 vol.% hydrogen peroxide for 30 min. The cleaned glass substrate was then rinsed with deionized (DI) water and dried at 200 °C for 10 min on a hotplate. The dehydrated glass substrate was first coated with 200 Å of chromium followed by 3000 Å of gold using an e-beam evaporator. The chromium/gold film later served as a seed layer of the electroplated nickel and silver for the anode and cathode, respectively. On the metallized glass substrate, a positive photoresist (Microposit S1813, Shipley Company, Marlboro, MA) was spin-coated at 3000 rpm for 30 s and the substrate was soft-baked at 90 °C for 4 min on a hotplate. The substrate was then exposed at a wavelength of 365 nm, in hard contact mode. After exposure, the exposed areas were developed in a developing solution (Microposit Developer 354, Shipley Company, Marlboro, MA) and then rinsed using DI water. After hard-baking at 110 °C for 15 min on a hotplate, etching was carried out. The gold layer (3000 Å) was first etched in a gold etchant (GE-8110, Transene Company, Danvers, MA), and the chromium layer (200 Å) was then etched in a chromium etchant (Cr-7, Cyantek Corp., Fremont, CA). On the patterned chromium/gold layer, the anode and cathode were selectively formed by electroplating nickel and silver, respectively. Nickel

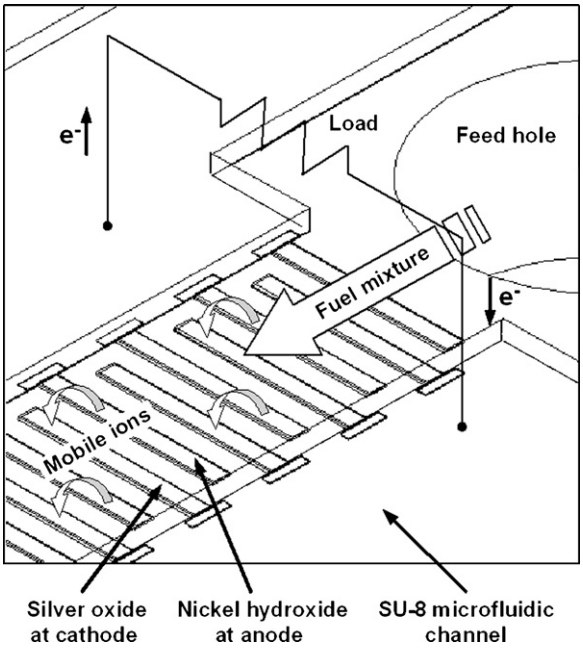


Fig. 7. Schematic illustration of interdigitated microelectrodes design of the microscale fuel cell.

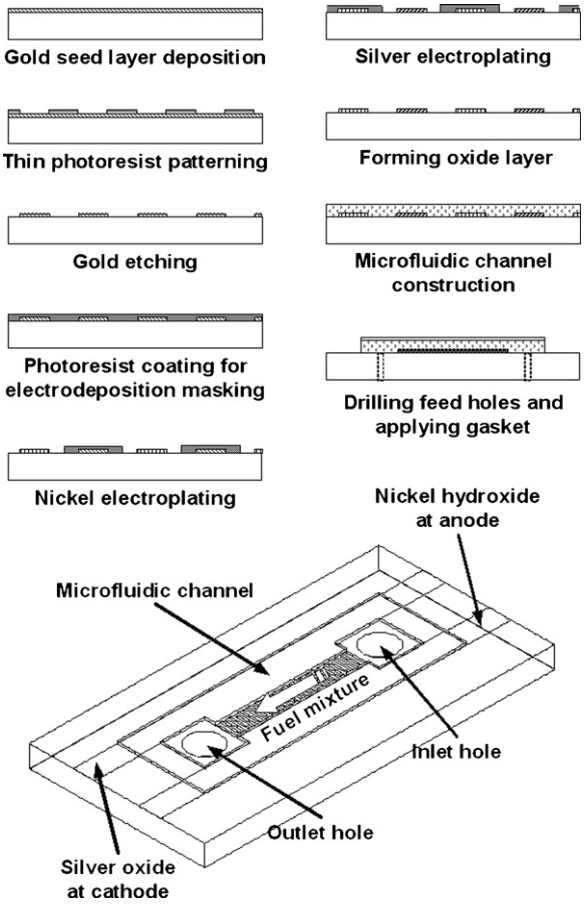


Fig. 8. Fabrication steps of the microscale fuel cell.

was first electroplated in the nickel sulfate-based electrolyte at a current density of 5 mA cm$^{-2}$ for 20 min. Silver was then electroplated using the commercially available silver electroplating solution (Cy-less Silver, Technic, Inc., Cranston, RI) at a current density of 3 mA cm$^{-2}$ for 15 min. During this process, two more photolithography steps were added to prevent cross-contamination. The cathode was covered by a positive photoresist while nickel electroplating for the anode, and the anode was also covered while silver electroplating for the cathode. The resulting thickness of both nickel and silver was 2 μm. Then, the electroplated nickel and silver were subjected to the oxide formation in an alkaline solution (1 M KOH). The electroplated nickel was voltammetry-cycled within −1.2 to 0.6 V with respect to a silver/silver chloride (Ag/AgCl) reference electrode in 1 M KOH at a scan rate of 10 mV s$^{-1}$ for 80 times, resulting in the electrochemically formed nickel hydroxide. During this treatment for 8 h, the electroplated silver was involuntarily immersed in 1 M KOH along with the electroplated nickel, resulting in the chemically formed silver oxide.

Next, a 100 μm-thick microfluidic channel was constructed on the interdigitated microelectrodes array by means of a negative thick photoresist (Nano SU-8 50, MicroChem, MicroChem Corp., Newton, MA) photolithography. A 100 μm-thick SU-8 was obtained by spinning for 30 s at 1000 rpm. The substrate was soft-baked at 97 °C for 90 min on a hotplate. The SU-8 photoresist was then exposed using the same lithography equipment as used for the S1813 photoresist in the previous step. The exposure dose was approximately 390 mJ cm$^{-2}$. Immediately after exposure, the SU-8 layer was subjected to a post-exposure bake at 97 °C for 20 min on a hotplate. Following post-exposure baking, the SU-8 photoresist was developed in a developing bath (Nano SU-8 Developer, MicroChem Corp., Newton, MA) for 10 min with mild agitation, then rinsed briefly with isopropyl alcohol (IPA), and finally dried with a gentle stream of nitrogen. Subsequently, the inlet and outlet holes of the microfluidic channel were drilled using a diamond drill bit and the substrate was diced for packaging. The fabrication steps are illustrated in Fig. 8. Fig. 9 shows the fabricated interdigitated microelectrodes and the assembled microscale fuel cell for testing.

### 4.3. The effect of distance between anode and cathode

Prior to the experiment of the fabricated microscale fuel cells, nickel hydroxide at anode was stabilized through the long-term fuel cell operation in conjunction with silver oxide at cathode. At a fuel flow rate of 10 μl min$^{-1}$, the output current was measured with a load resistance of 100 Ω for 4 h. Despite different designs, the output current continuously decreased for 2–3 h and then settled at stabilized values, as previously observed with the macroscale fuel cell. It is believed that the observed decline in the output current was caused by the aging effect of nickel hydroxide at the anode [32,33], as previously explained with the macroscale fuel cell.

After stabilizing the catalyst in the microscale fuel cells, the output voltage and current were measured with various external loads. As shown in Fig. 10, not only at the macroscale level but also at the microscale level, the maximum output power density was dependent on the distance between the anode and cathode. Considering the presence of reacting species moving

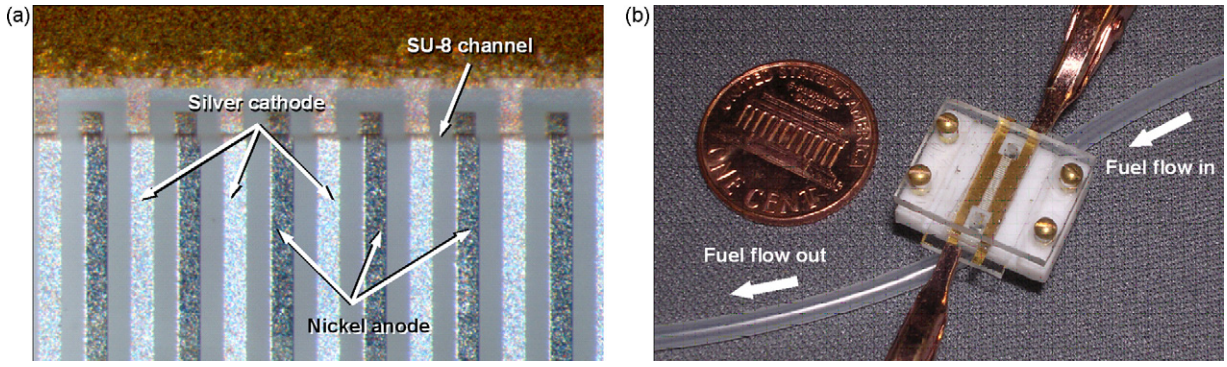


Fig. 9. Microscale fuel cell: (a) microphotograph of the fabricated interdigitated microelectrodes with 50 μm width and spacing and (b) photograph of the packaged fuel cell for testing. The packaged size is 15 mm × 12 mm × 5 mm.

between the anode and cathode, it is believed that a shorter distance between the anode and cathode leads to a faster transport time of reacting species and then more electrochemical reactions occur at a given time developing a higher fuel cell output current. Since the developed microscale fuel cell does not require a proton exchange membrane or a laminar flow control, it is feasible to further reduce the diffusion length between the anode and cathode for a higher output power per a given device size.

### 4.4. The effect of fuel mixture flow rate

As an another means to control the transport time of reacting species moving between the anode and cathode, different

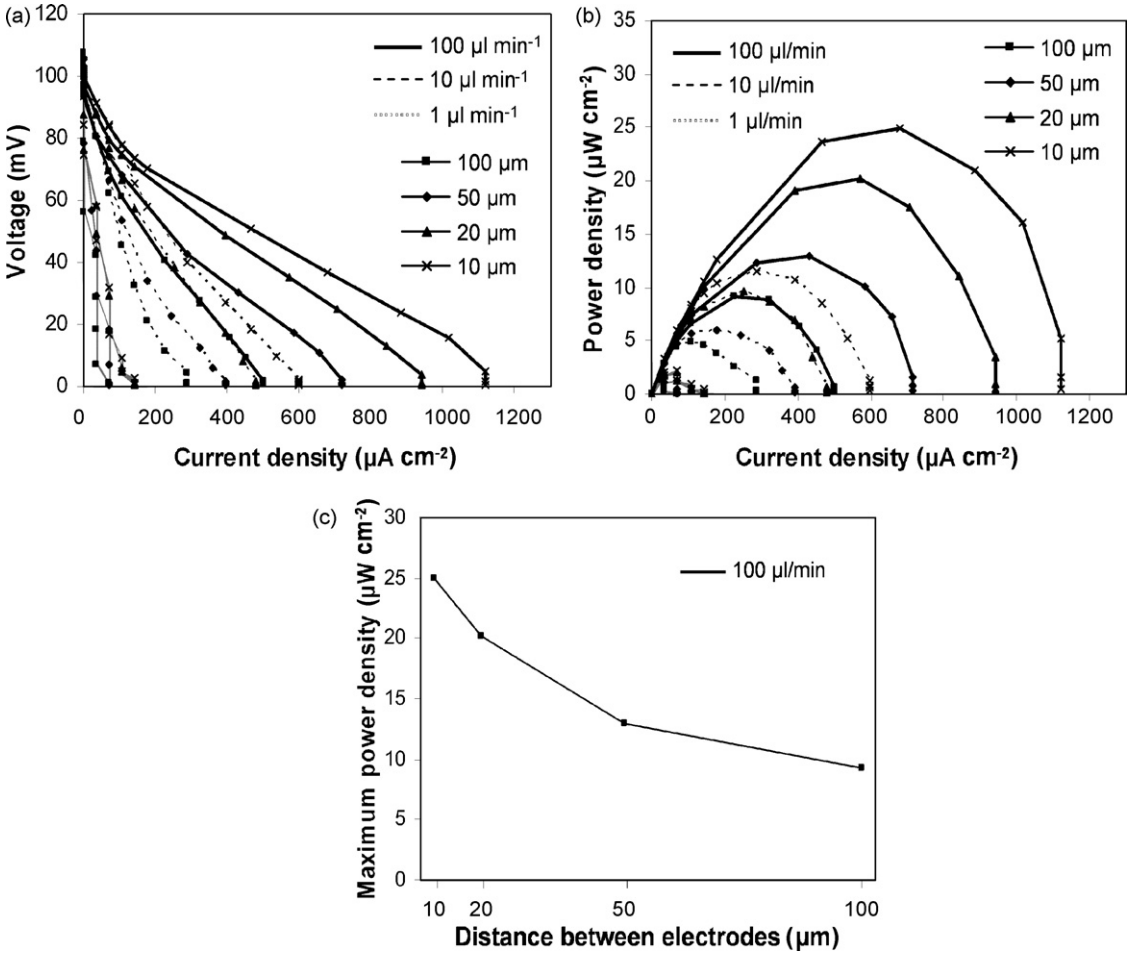


Fig. 10. Effect of distance between anode and cathode on the fuel cell output: (a) the output voltage vs. the output current density, (b) the output power density vs. the output current density, and (c) the maximum output power density vs. the distance between electrodes. For comparison, three different fuel mixture flow rates are present. The output voltage and current were measured with various external loads. For each design, three microscale fuel cell samples were tested. Three sets of the fuel cell averaged and then plotted. The fuel mixture of 0.2 M KOH + 2 M $CH_3OH$ + 0.05 M $H_2O_2$ was supplied at a rate of 10 μl $min^{-1}$. Temperature was 22.5 °C.

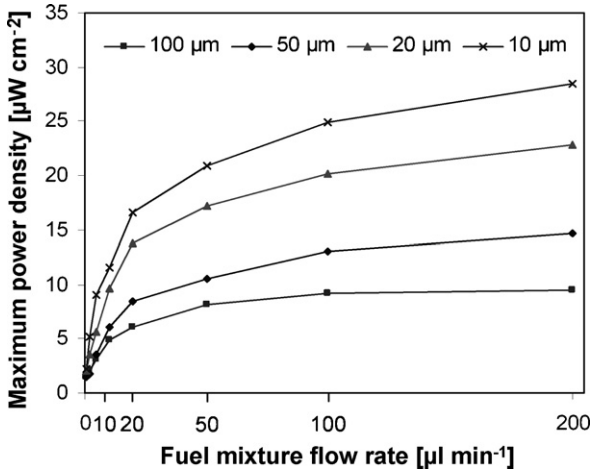


Fig. 11. Effect of fuel mixture flow rate on the fuel cell output power. For comparison, four different designs are present. The output voltage and current were measured with various external loads. For each flow rate, three microscale fuel cell samples were tested. Three sets of the fuel cell output were averaged and then plotted. The fuel mixture of 0.2 M KOH + 2 M $CH_3OH$ + 0.05 M $H_2O_2$ was supplied. Temperature was 22.5 °C.

fuel mixture flow rates were applied to the microscale fuel cell. In this experiment, flow rates of 1, 2, 5, 10, 20, 50, 100, and 200 μl $min^{-1}$ were tested. Except for the fuel mixture flow rate, other test conditions were consistent with the previous experiment. The output voltage and current were measured with different external loads as a function of the fuel mixture flow velocity. A flow velocity can be calculated from the flow rate applied and the cross-sectional area of the microfluidic channel used. As shown in Fig. 11, as the flow rate increased, the maximum output power density increased. A maximum output power density of 2.28, 11.67, and 25.44 μW $cm^{-2}$ was extractable from the 10 μm design at a flow rate of 1, 10, and 100 μl $min^{-1}$, respectively. Like a shorter distance between electrodes, a higher fuel mixture flow rate could enable a shorter transport time of reacting species moving between the anode and cathode. It is believed that more electrochemical reactions would take place at a given time and a greater output current could develop in the end. Despite insufficient evidence, it is also believed that fuel and oxidant molecules as well as mobile ions are influenced by the forced flow of fuel mixture. Thus, the number of fuel and/or oxidant species available at the surface of an electrode might increase and the electrochemical reaction rate could also increase.

### 4.5. Discussion

The developed fuel cells exhibit low power output because of the mild catalysts on the anode and cathode and cross-reactions of fuel and oxidant. Mild catalysts were necessary to minimize the undesired cross-reactions caused by the membraneless structure and, as a result, the obtained output power was lower than reported liquid-based microscale fuel cells. Besides, fuel and oxidant was not segregated unlike laminar flow-based microscale fuel cells, which resulted in undesired cross-reactions. For the anode and cathode catalysts, hydroxyl ions were essential to be electroactive for the redox reactions. In the presence of hydroxyl ions, nickel hydroxide catalyzed the anodic oxidation of methanol and silver oxide catalyzed the cathodic reduction of hydrogen peroxide. However, hydrogen peroxide was also reactive at nickel hydroxide, while methanol was insensitive at silver oxide, which indicates that cross-reactions could occur during fuel cell operation. Relatively active hydrogen peroxide and hydroxyl ion affected the stability of the anode and cathode, and therefore a stabilization process was required before the initial use of the fuel cells. Three to 4 h of continuous operation in a fuel mixture must have been carried out for the anode and cathode. Once treated, the performance of the fuel cells was stable for the repeated use over 6 months.

In spite of low output power, the developed fuel cells can easily be stackable and integrated in a given volume without a complicated flow control scheme. Only bulky component of the stackable fuel cells would be the substrate for the electrodes, which can be as thin as few tens of micrometers. Fuel flow does not need to be laminar so the fuel flow rate and the fuel channel structure can be flexibly determined. Although the developed fuel cells are not practical at the current stage due to the power output, the obtained results in this work show a feasibility of high density stackable fuel cells with non-noble catalysts and a simple structure.

## 5. Conclusions

The methanol and hydrogen peroxide fuel cell was successfully developed and demonstrated using non-noble catalysts in an alkaline solution. Based on a membraneless structure in this fuel cell, a shorter distance between anode and cathode was shown to generate a higher output power. Further developing this distance effect, the microscale fuel cell was constructed, which allowed microscale lengths for reactant diffusion and expedited the electrochemical reactions. With a fuel mixture flow rate of 200 μl $min^{-1}$, a maximum output power density of 28.73 μW $cm^{-2}$ was extracted from the 10 μm design, which was nearly three times higher than the 100 μm design. This consequence can be interpreted that a shorter distance between anode and cathode would lead to a faster transport time of reacting species, which results in more electrochemical reactions at a given time and thus a higher output power. The advantages of the microscale fuel cell developed in this work, particularly over previously reported microscale direct methanol fuel cells, are no proton exchange membrane, inexpensive catalysts, no laminar flow control in microchannels, and a simple planar structure. Furthermore, the simple structure could make it possible to integrate a large number of the microscale fuel cells in a given volume for a higher volumetric power density. Due to the simple structure of the developed fuel cells, the anode and cathode can be arranged on the same plane without a proton exchange membrane, which enables that the fuel cell dimensions can be flexibly adjusted to meet specific design needs for the applications of microfluidic systems and portable power sources.

## Acknowledgments

This research was supported in part by Louisiana State University Council on Research, the Center for Computation and Technology at Louisiana State University, and Louisiana Board of Regents Research Competitiveness Subprogram under contract LEQSF(2004-07)-RD-A-06.

## References

[1] G. Hoogers, Fuel Cell Technology Handbook, CRC Press, Boca Raton, 2002.
[2] J.-M. Tarascon, M. Armand, Nature 414 (2001) 359–367.
[3] S.K. Dhar, S.R. Ovshinsky, P.R. Gifford, D.A. Corrigan, M.A. Fetcenko, S. Venkatesan, J. Power Sources 65 (1997) 1–7.
[4] H.L. Maynard, J.P. Meyers, J. Vac. Sci. Technol. B 20 (2002) 1287–1297.
[5] C.K. Dyer, J. Power Sources 106 (2002) 31–34.
[6] R.F. Service, Science 296 (2002) 1222–1224.
[7] J. Larminie, A. Dicks, Fuel Cell Systems Explained, 2nd ed., John Wiley & Sons Ltd., Chichester, 2003.
[8] S.C. Kelley, G.A. Deluga, W.H. Smyrl, J. Am. Inst. Chem. Eng. 48 (2002) 1071–1082.
[9] S.R. Narayanan, T.I. Valdez, F. Clara, Proceedings of the 199th Meeting on Direct Methanol Fuel Cell, Electrochemical Society, 2001, pp. 254–263.
[10] H. Chang, J.R. Kim, J.H. Cho, H.K. Kim, K.H. Choi, Solid State Ionics 148 (2002) 601–606.
[11] J. Bostaph, R. Koripella, A. Fisher, D. Zindel, J. Hallmark, Proceedings of the 199th Meeting on Direct Methanol Fuel Cell, Electrochemical Society, 2001, pp. 892–895.
[12] G.Q. Lu, C.Y. Wang, T.J. Yen, X. Zhang, Electrochim. Acta 49 (2004) 821–828.
[13] S.-C. Yao, X. Tang, C.-C. Hsieh, Y. Alyousef, M. Vladimer, G.K. Fedder, C.H. Amon, Energy 31 (2006) 636–649.
[14] J.-W. Choi, W. Sung, Technical Digest of the 13th International Conference on Solid-State Sensors, Actuators, and Microsystems, 2005, pp. 1852–1855.
[15] S.M. Haile, Acta Mater. 51 (2003) 5981–6000.
[16] D.-S. Meng, T. Cubaud, C.-M. Ho, C.-J. Kim, Technical Digest of Solid-State Sensor, Actuator and Microsystems Workshop, 2004, pp. 141–144.
[17] E.R. Choban, L.J. Markoski, A. Wieckowski, P.J.A. Kenis, J. Power Sources 128 (2004) 54–60.
[18] E.R. Choban, J.S. Spendelow, L. Gancs, A. Wieckowski, P.J.A. Kenis, Electrochim. Acta 50 (2005) 5390–5398.
[19] J.L. Cohen, D.J. Volpe, D.A. Westly, A. Pechenik, H.D. Abruna, Langmuir 21 (2005) 3544–3550.
[20] M.-H. Chang, F. Chen, N.-S. Fang, J. Power Sources 159 (2006) 810–816.
[21] C. Iwakura, H. Tamura, T. Ishino, J. Electrochem. Soc. Jpn. 36 (1968) 107–113.
[22] G. Bianchi, G. Caprioglio, F. Mazza, T. Mussini, Electrochim. Acta 4 (1961) 232–241.
[23] C. Iwakura, Y. Matsuda, H. Tamura, Electrochim. Acta 16 (1971) 471–477.
[24] M. Honda, T. Kodera, H. Kita, Electrochim. Acta 28 (1983) 727–733.
[25] E.R. Savinova, S. Wasle, K. Doblhofer, Electrochim. Acta 44 (1998) 1341–1348.
[26] D.J. Brodrecht, D.N. Prater, J.J. Rusek, Novel Fuel Cells Using Hydrogen Peroxide, Tech. Rep., Swift Enterprises Ltd., West Lafayette, IN, 2001.
[27] W.T. Hess, Kirk–Othmer Encyclopedia of Chemical Technology, 4th ed., John Wiley & Sons Ltd., New York, 1995.
[28] D.N. Prater, J.J. Rusek, Appl. Energy 74 (2003) 135–140.
[29] A. Nagy, G. Mestl, Appl. Catal. A: Gen. 188 (1999) 337–353.
[30] M. Qian, M.A. Liauw, G. Emig, Appl. Catal. A: Gen. 238 (2003) 211–222.
[31] M. Fleischmann, K. Korinek, D. Pletcher, J. Electroanal. Chem. 31 (1971) 39–49.
[32] J. Taraszewska, G. Roslonek, J. Electroanal. Chem. 364 (1994) 209–213.
[33] A.A. El-Shafei, J. Electroanal. Chem. 471 (1999) 89–95.
[34] M.A. Abdel Rahim, R.M. Abdel Hameed, M.W. Khalil, J. Power Sources 134 (2004) 160–169.
[35] P. Oliva, J. Leonardi, J.F. Laurent, C. Delmas, J.J. Braconnier, M. Figlarz, F. Fievet, A. de Guibert, J. Power Sources 8 (1982) 229–255.
[36] P.V. Kamath, M. Dixit, L. Indira, A.K. Shukla, V.G. Kumar, N. Munichandraiah, J. Electrochem. Soc. 141 (1994) 2956–2959.
[37] M.-S. Kim, T.-S. Hwang, K.-B. Kim, J. Electrochem. Soc. 144 (1997) 1537–1543.
[38] S.B. Hall, E.A. Khudaish, A.L. Hart, Electrochim. Acta 43 (1997) 579–588.
[39] S.B. Hall, J.J. Nairn, E.A. Khudaish, Phys. Chem. Chem. Phys. 3 (2001) 4566–4571.
[40] C.G. Granqvist, Handbook of Inorganic Electrochromic Materials, Elsevier, Amsterdam, 1995.
[41] A. Soto, PhD Dissertation, Uppsala University, Sweden, 2004.